Strong thermalization of the two-component Bose-Hubbard model at finite temperatures

J. M. Zhang,[1,2] C. Shen,[2] and W. M. Liu[1]

[1]*Institute of Physics, Chinese Academy of Sciences, Beijing 100080, China*

[2]*Department of Physics, University of Michigan, Ann Arbor, Michigan 48109, USA*

(Received 9 January 2011; revised manuscript received 26 October 2011; published 27 January 2012)

We study thermalization of a two-component Bose-Hubbard model by exact diagonalization. Initially, the two components do not interact and are both at equilibrium but with different temperatures. As the onsite intercomponent interaction is turned on, perfect thermalization occurs. Remarkably, not merely those simple "realistic" physical observables thermalize but even the density matrix of the *whole* system—the time-averaged density matrix of the system can be well approximated by that of a canonical ensemble. We also discuss how symmetry of the quenched Hamiltonian affects the level spacing distribution and thermalization of the system.

DOI: 10.1103/PhysRevA.85.013637 PACS number(s): 67.85.−d, 05.70.Ln, 05.30.Jp

I. INTRODUCTION

For an isolated system, how and in which sense thermal equilibrium is reached from an initially nonequilibrium state, or even whether it can be reached or not, has long been a problem [1]. A modern investigation came with the Fermi-Pasta-Ulam simulation as soon as the electric computer was available [2]. The surprising result was that the system exhibited a long-time periodic behavior without any sign of ergodicity, which was later ascribed to the integrability of the model in the continuum limit [3]. More recently, the problem revived again because of the possibility of using ultracold atoms to address it experimentally [4]. Many different models, integrable [4–6] or nonintegrable [7–10], are investigated. For those models integrable, as expected, no thermalization, or at least no thermalization in the usual Gibbs-ensemble sense is observed [4–6]. What is unexpected is that, even for some nonintegrable models [7–9], thermalization does not occur, at least at finite sizes and at zero temperature. Moreover, even if thermalization does show up [9,10], it thermalizes only in the sense that some physical observables relax to the predicted values of a microcanonical or canonical ensemble—yet the time-averaged density matrix itself shares little feature with a microcanonical or canonical ensemble (an exception is [11], where signature of this is observed). Therefore, the system thermalizes in a weak or pragmatic sense, since it is the few simple observables that are readily measured and thus of most concern that thermalize.

In this paper, we investigate thermalization of the two-component Bose-Hubbard model, which is known as nonintegrable (see Fig. 2 below). Though at zero temperature the system shows no sign of thermalization at the finite sizes accessible, at finite temperatures we do find that in some regimes the model thermalizes very well at a finite size. Remarkably, unlike previous works, it is not only some simple observables that thermalize but even the time-averaged density matrix (of the *whole* system) itself, which can be well approximated by a canonical ensemble density matrix. The motivation is to simulate the everyday experience that two objects initially at different temperatures, when brought in contact, equilibrate eventually as a whole. This textbook scenario is familiar to everyone and deserves a first-principle investigation. Here, "first principle" means we are allowed to explore freely without the restriction of empirical assumptions and possibly go beyond standard statistical mechanics [12]. Specifically, our approach will be primarily numerical exact diagonalization, and in spirit it is very much like the Fermi-Pasta-Ulam simulation.

Here, the two species of bosons act as the two objects. It is assumed that initially each component is at equilibrium in themselves and at some finite but different temperatures and there is no interaction between them. Then at time $t = 0$, the intercomponent interaction is switched on and the subsequent evolution is studied. Note that the two-component Bose-Hubbard model we choose has a desirable property. That is, it is potentially realizable experimentally using cold atoms in optical lattices. In particular, the intercomponent interaction can be controlled with Feshbach resonance.

This paper is organized as follows. In Sec. II, the model is defined and the principal object of study—the time-averaged density matrix $\bar{\rho}$ is introduced. In passing, the numerical method is explained in detail. In Sec. III, we focus on the time-averaged density matrix $\bar{\rho}$ (a sector of it in some quasimomentum space actually). We will try to characterize $\bar{\rho}$ in various means, using various criterions. The central observation will be that $\bar{\rho}$ can be well approximated by the canonical ensemble density matrix ρ_c, which is of the same energy as $\bar{\rho}$, in some regime. It is also found that $\bar{\rho}$ is intricately structured in the presence of symmetry. The good agreement between $\bar{\rho}$ and ρ_c constitutes a highly nontrivial fact and its implications are discussed in Sec. IV. The conclusions are presented in Sec. V.

II. THE MODEL AND THE BASIC APPROACH

The Hamiltonian is ($\hbar = k_B = 1$) $\hat{H}_t = \hat{H}_a + \hat{H}_b + \theta_t \hat{H}_{ab}$, where $\hat{H}_{a,b}$ are Hamiltonians of components a and b, respectively. Explicitly,

$$\hat{H}_a = -J_a \sum_{m=1}^{M} (\hat{a}_m^\dagger \hat{a}_{m+1} + \text{H.c.}) + \frac{U_a}{2} \sum_{m=1}^{M} \hat{a}_m^\dagger \hat{a}_m^\dagger \hat{a}_m \hat{a}_m,$$

and $\hat{H}_a \leftrightarrow \hat{H}_b$ as $a \leftrightarrow b$. Here, M is the number of sites and periodic boundary condition is assumed. The intercomponent interaction is of the on-site type: $\hat{H}_{ab} = U_{ab} \sum_{m=1}^{M} \hat{a}_m^\dagger \hat{a}_m \hat{b}_m^\dagger \hat{b}_m$. The control function is defined as $\theta_{t<0} = 0$ while $\theta_{t\geqslant 0} = 1$. By assumption, the initial density matrix of the whole system is

$\rho(0)=\rho_a(0)\otimes\rho_b(0)$, where the initial density matrices of the two components are ($\alpha=a,b$)

$$\rho_\alpha(0)=\frac{1}{Z_\alpha}\sum_{j=1}^{D_\alpha}e^{-\beta_\alpha E_\alpha^j}|j\rangle_\alpha\langle j|. \tag{1}$$

Here, β_α is the inverse temperature of the component α, $|j\rangle_\alpha$ denotes the jth eigenstate of $\hat{H}_\alpha$ with eigenvalue E_α^j, and $Z_\alpha=\sum_{j=1}^{D_\alpha}e^{-\beta_\alpha E_\alpha^j}$ is the partition function. The dimension of the Hilbert space $\mathcal{H}_\alpha$ of component α is $D_\alpha=\frac{(M+N_\alpha-1)!}{(M-1)!N_\alpha!}$, with N_α being the total atom number of component α.

Now turn on the interaction. Denote the nth eigenstate (with eigenvalue E_n) of the quenched Hamiltonian $\hat{H}_{t\geqslant 0}$ as $|\psi_n\rangle$. The density matrix at an arbitrary time later is formally $\rho(t)=\sum_{n,l=1}^{D}\langle\psi_n|\rho(0)|\psi_l\rangle e^{-i(E_n-E_l)t}|\psi_n\rangle\langle\psi_l|$, where $D=D_aD_b$ is the dimension of the full Hilbert space $\mathcal{H}=\mathcal{H}_a\otimes\mathcal{H}_b$. At this point, the time-averaged density matrix is defined as

$$\begin{aligned}\bar{\rho}&\equiv\lim_{\tau\to\infty}\frac{1}{\tau}\int_0^\tau dt\rho(t)\\&=\sum_{n,l=1;E_n=E_l}^{D}\langle\psi_n|\rho(0)|\psi_l\rangle|\psi_n\rangle\langle\psi_l|.\end{aligned} \tag{2}$$

The operator $\bar{\rho}$ is of significant relevance for our purpose for multiple reasons. First, it is observable-free. Second, the time-averaged value of an arbitrary operator is given simply by $\overline{\langle\hat{O}\rangle}\equiv\lim_{\tau\to\infty}\frac{1}{\tau}\int_0^\tau \mathrm{tr}[\rho(t)\hat{O}]dt=\mathrm{tr}(\bar{\rho}\hat{O})$. As proven in Ref. [13], for many observables, the fluctuation of $\langle\hat{O}\rangle$ around its average value shrinks exponentially with the system size [14]. Thus, the dynamics of $\langle\hat{O}\rangle$ is to a good extent captured by $\overline{\langle\hat{O}\rangle}$. Third, the process of averaging over time is a process of relaxation in the sense that the entropy associated with $\bar{\rho}$ is definitely no less than that with $\rho(t)$, i.e., $S(\bar{\rho})\geqslant S(\rho(t))=S(\rho(0))$. This is a corollary of the Klein inequality [15] and is reasonable since $\rho(0)$ contains all the information of $\bar{\rho}$ while the inverse is invalid.

We note that $\hat{H}_t$ is invariant under the simultaneous translations $(\hat{a}_m,\hat{b}_m)\to(\hat{a}_{m+1},\hat{b}_{m+1})$. Especially, the initial Hamiltonian $\hat{H}_{t<0}=\hat{H}_a+\hat{H}_b$ is invariant under the two translations individually. This implies the conservation of quasimomentum(a) (QM). The QM of component a is defined as

$$q_a=\sum_{k=0}^{M-1}k\hat{a}_k^\dagger\hat{a}_k\pmod M, \tag{3}$$

where $\hat{a}_k^\dagger=\frac{1}{\sqrt{M}}\sum_m e^{im2\pi k/M}\hat{a}_m^\dagger$ is the creation operator of an atom in the kth Bloch state. Similar operators are defined for component b. Our strategy is then to transform to the QM space. We decompose the total Hilbert space $\mathcal{H}$ into M subspaces according to the total QM $q=q_a+q_b$, $\mathcal{H}=\oplus_{q=0}^{M-1}\mathcal{H}^{(q)}$, which are further decomposed according to the QM of the two components (q_a,q_b), $\mathcal{H}^{(q)}=\oplus_{q_a=0}^{M-1}\mathcal{H}_a^{(q_a)}\otimes\mathcal{H}_b^{(q-q_a)}$. The Hamiltonian and density matrix are always block-diagonal with respect to the q subspaces, $\hat{H}_t=\oplus_{q=0}^{M-1}\hat{H}_t^{(q)}$ and $\rho(t)=\oplus_{q=0}^{M-1}\rho^{(q)}(t)$. In particular, the initial density matrix can be decomposed finer as $\rho^{(q)}(0)=\oplus_{q_a=0}^{M-1}\rho_a^{(q_a)}(0)\otimes\rho_b^{(q-q_a)}(0)$ with $\rho_\alpha^{(q_\alpha)}\in\mathcal{H}_\alpha^{(q_\alpha)}$, since $\hat{H}_{t<0}^{(q)}$ can be decomposed similarly. In each q subspace, generally there is no degeneracy between the eigenstates $\{|\psi_n\rangle\}$, therefore, the $\bar{\rho}$ in each q subspace is simply the diagonal part of the initial density matrix in the $\{|\psi_n\rangle\}$ representation, i.e., $\langle\psi_n|\bar{\rho}^{(q)}|\psi_l\rangle=\delta_{nl}\langle\psi_n|\rho^{(q)}(0)|\psi_l\rangle$.

Here, some remarks are in order. First, technically we use the exact diagonalization algorithm in Ref. [16]. To be specific, we work in the momentum representation and rewrite the Hamiltonian $\hat{H}_t$ in terms of the operators $\hat{a}_k$ and $\hat{b}_k$. We then enumerate all the Fock states in the q subspace and set up the matrix corresponding to $\hat{H}_t^{(q)}$ in this basis. These are done using the tricks in Ref. [16]. Once the Hamiltonian matrix is diagonalized completely, all quantities can be calculated easily. It should be stressed that we impose no cutoff on the occupation number on each site. That is, our numerical simulation is completely exact. Second, it should be mentioned that for some quantities [e.g., $\langle\hat{a}_k^\dagger\hat{a}_k\rangle$] studied below, we should have averaged over all the q subspaces. However, in this paper we do not do so, because the system behaves quantitatively similar in all the q subspaces [see Fig. 1(c)]. This fact is reasonable and is even expected in the thermodynamic limit. The reason is that the value of q can be changed from one to another by simply changing the quasimomentum of a *single* atom—a process expected to be of little influence on the thermodynamics of the system. Given that a single q subspace captures the overall behavior well, we shall focus on a specific q subspace ($q=1$) and take the normalization $\mathrm{tr}[\rho^{(q)}(t)]=1$.

III. CHARACTERIZATION OF $\bar{\rho}$

As mentioned above, our motivation is to study the relaxation dynamics of the initially nonequilibrium system. A natural question is, then, what $\bar{\rho}^{(q)}$ is like. The following subsections are devoted to various aspects of it.

A. Canonical distribution

As revealed by Fig. 1, at least in some regimes, the time-averaged density matrix $\bar{\rho}^{(q)}$ has a strong characteristic of a canonical ensemble [17]. In each panel, the occupations $p_n=\langle\psi_n|\bar{\rho}^{(q)}|\psi_n\rangle$ on the eigenstates are plotted versus the eigenvalues E_n. It is amazing that most of the points cling close to a straight line except at the ends of the spectrum, and the straight line is actually the prediction of a canonical ensemble,

$$\rho_c^{(q)}(\beta_f)\equiv\frac{e^{-\beta_f\hat{H}_{t>0}^{(q)}}}{\mathrm{tr}\left(e^{-\beta_f\hat{H}_{t>0}^{(q)}}\right)}, \tag{4}$$

with the same energy as $\bar{\rho}^{(q)}$, i.e., $\bar{E}\equiv\mathrm{tr}(\hat{H}_{t>0}^{(q)}\bar{\rho}^{(q)})=\mathrm{tr}[\hat{H}_{t>0}^{(q)}\rho_c^{(q)}(\beta_f)]$. The situation improves if the initial temperatures $1/\beta_{a,b}$ are increased and worsens if they are decreased. The relatively bad agreement between $\bar{\rho}^{(q)}$ and $\rho_c^{(q)}$ at the edges of the spectrum or at low temperatures is expected, since a finite system with few-body and finite-range interactions is not chaotic at the edges of the spectrum [18].

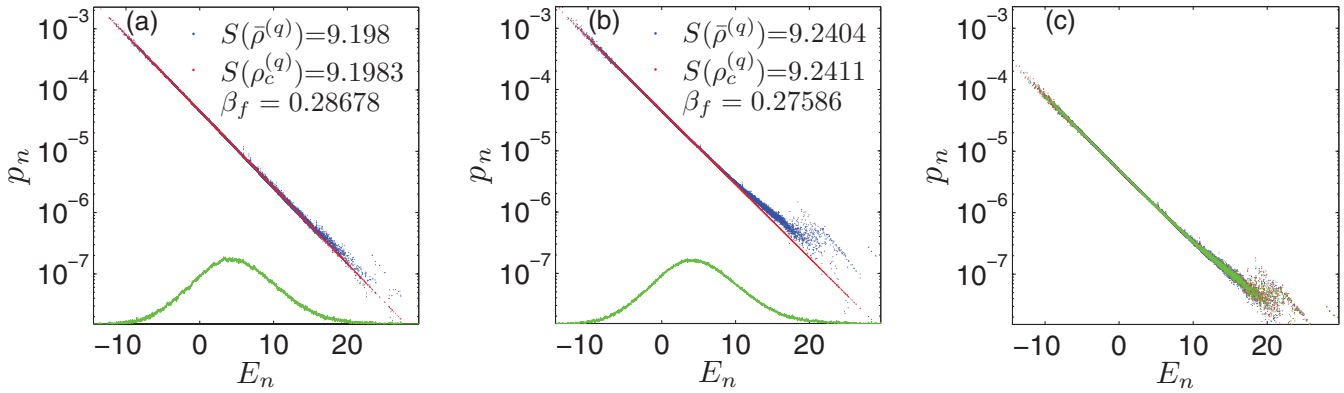

FIG. 1. (Color online) (a) and (b): Diagonal elements of $\bar{\rho}^{(q)}$ (blue dots) and $\rho_c^{(q)}$ (red dots) versus the eigenvalues E_n. The parameters are $(N_a,N_b,M,q) = (4,4,9,1)$, $(J_a,J_b,U_a,U_b) = (1,1,2,2)$, $(\beta_a,\beta_b) = (0.2,0.4)$, and $U_{ab} = 0.5$ in (a); $U_{ab} = 1$ in (b). The dimension of the q subspace is $D^{(q)} = 27{,}225$. The green lines depict the coarse-grained density of states of $\hat{H}_{t>0}^{(q)}$ (just for reference, not corresponding to the vertical axes). The inverse temperature β_f and the entropies of $\bar{\rho}^{(q)}$ and $\rho_c^{(q)}$ are shown in the inserts. (c) is an extension of (b), where three q subspaces ($q = 0$, blue dots; $q = 1$, red dots; $q = 2$, green dots) are investigated. The blue and red dots are hardly visible because they are covered by the green dots. Note that in (a) and (b) we use $\mathrm{tr}(\bar{\rho}^{(q)}) = 1$, while in (c) $\mathrm{tr}(\bar{\rho}) = 1$.

Besides Fig. 1, we have explored the parameter space extensively. The observation is that when the J's and U's are comparable, i.e., when the model is far from the integrable limits, results similar to Fig. 1 can occur. Of course, the fitting is not always as good as in Fig. 1. In the low temperature or unbalanced case ($|\beta_a - \beta_b|$ large), the fitting worsens (e.g., see Fig. 4). We will come back to this point later in Sec. IV.

Having the eigenvalues of $\hat{H}_{t>0}^{(q)}$ solved numerically, we have also studied its level spacing statistics. The results are shown in Fig. 2. There the two panels correspond to the first two panels of Fig. 1 one to one. It is apparent that the Hamiltonian $\hat{H}_{t>0}^{(q)}$, in the specific parameters, belongs to the Gaussian orthogonal ensemble (GOE) universal class. This proves that the model in question is generically nonintegrable as expected.

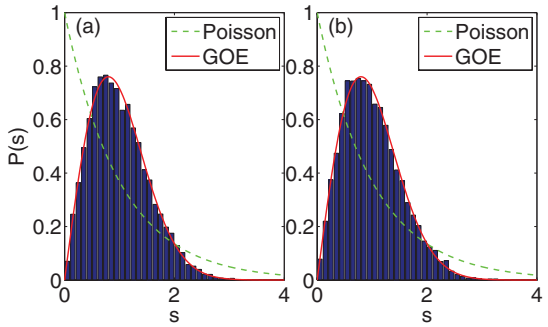

FIG. 2. (Color online) Level spacing distribution of the Hamiltonian $\hat{H}_{t>0}^{(q)}$. Each panel corresponds to that in Fig. 1, respectively, with the same parameters. In each panel, the green dashed line and the red solid line correspond to the Poisson distribution $P_P(s) = \exp(-s)$ and Wigner-Dyson distribution $P_{\mathrm{WD}}(s) = \frac{\pi s}{2}\exp(-\pi s^2/4)$ of a Gaussian orthogonal ensemble (GOE), respectively. We employ the unfolding procedure in [19]. Note that due to the symmetric parameters ($J_a = J_b$, $U_a = U_b$, $N_a = N_b$), the Hamiltonian is invariant under the exchange $a \leftrightarrow b$. Therefore, only eigenstates even under the exchange are counted.

B. The weak coupling limit of $U_{ab} \to 0$

Here, the weak intercomponent interaction limit $U_{ab} \to 0$ is of special interest [17]. On one hand, when $U_{ab} = 0$, the eigenvalues of $\hat{H}_{t>0}^{(q)}$ are direct sums of those of $\hat{H}_a^{(q_1)}$ and $\hat{H}_b^{(q_2)}$ ($q_1 + q_2 = q$), and thus the level spacing statistics should be Poisson. Therefore, as U_{ab} increases from zero, there should be a crossover from the Poisson distribution to the GOE distribution as shown in Fig. 2. On the other hand, in the symmetric cases (i.e., $J_a = J_b$, $U_a = U_b$, and $N_a = N_b$) as in Fig. 1, for U_{ab} small enough, the degeneracy between $|\phi_m^{q_1}\rangle_a|\phi_n^{q_2}\rangle_b$ and $|\phi_n^{q_2}\rangle_a|\phi_m^{q_1}\rangle_b$ is lifted (if they are different; otherwise, only the plus sign should be taken) to form eigenstates of $\hat{H}_{t>0}^{(q)}$,

$$|q_1q_2mn;\pm\rangle = \frac{1}{\sqrt{2}}\left(|\phi_m^{q_1}\rangle_a|\phi_n^{q_2}\rangle_b \pm |\phi_n^{q_2}\rangle_a|\phi_m^{q_1}\rangle_b\right) \tag{5}$$

with eigenvalues approximately $E_m^{q_1} + E_n^{q_2}$. Here, $|\phi_m^{q_i}\rangle_\alpha$ ($\alpha = a,b$ and $i = 1,2$) is the mth eigenstate of $\hat{H}_\alpha^{(q_i)}$ with eigenvalue $E_m^{q_i}$. Note that in the symmetric case, $E_m^{q_i}$ is independent of α. Moreover, the populations on $|q_1q_2mn;\pm\rangle$ are

$$p_\pm = \frac{1}{2Z}\left(e^{-\beta_a E_m^{q_1} - \beta_b E_n^{q_2}} + e^{-\beta_a E_n^{q_2} - \beta_b E_m^{q_1}}\right), \tag{6}$$

where Z is a normalization factor (or partition function). It is easy to show that

$$\ln(p_\pm) \geqslant -\tfrac{1}{2}(\beta_a + \beta_b)\left(E_m^{q_1} + E_n^{q_2}\right) - \ln Z, \tag{7}$$

and ($\beta_a < \beta_b$)

$$\ln(p_\pm) \leqslant -\beta_b\left(E_m^{q_1} + E_n^{q_2}\right) + (\beta_b - \beta_a)E_u - \ln Z, \tag{8a}$$

$$\ln(p_\pm) \leqslant -\beta_a\left(E_m^{q_1} + E_n^{q_2}\right) - (\beta_b - \beta_a)E_l - \ln Z, \tag{8b}$$

where $E_{l,u}$ are the lower and upper bounds of $E_m^{q_1}$. The equalities in Eqs. (7), (8a), and (8b) are approached, respectively,

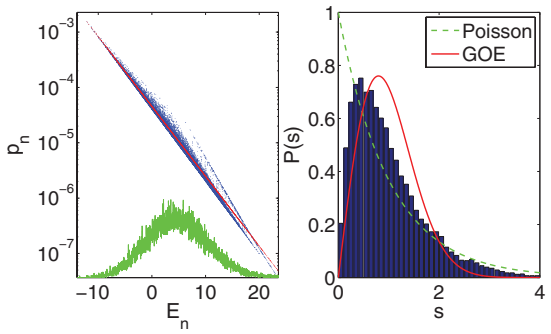

FIG. 3. (Color online) Left panel: diagonal elements of $\bar{\rho}^{(q)}$ (blue dots) and $\rho_c^{(q)}$ (red dots) versus the eigenvalues E_n. Note that the blue dots are sharply bounded by a triangle, the slopes of whose boundaries are $-\beta_a$, $-\beta_b$, and $-\frac{1}{2}(\beta_a+\beta_b)$, respectively. Right panel: level spacing distribution of the Hamiltonian $\hat{H}_{t>0}^{(q)}$, processed in the same way as in Fig. 2. The parameters are the same as in Fig. 1 and Fig. 2, except that $U_{ab}=0.025$.

when $(E_m^{q_1}-E_n^{q_2})$ approaches zero, when $\min(E_m^{q_1},E_n^{q_2})=E_l$, and when $\max(E_m^{q_1},E_n^{q_2})=E_u$. It is interesting that the three boundaries form a triangle with slopes $-\frac{1}{2}(\beta_a+\beta_b)$, $-\beta_b$, and $-\beta_a$, respectively.

In Fig. 3, we have studied the case with $U_{ab}=0.025$, which is much smaller than the J's and U's. The two points above are verified excellently. In Fig. 3(b), the level spacing statistics are apparently between the Poisson and the Wigner-Dyson statistics, and in Fig. 3(a), the triangle envelope is clearly visible.

Here again some remarks are in order. First, though the discussion above is very instructive, one should note that the phenomena associated with the $U_{ab}\to 0$ limit are finite-size effects essentially. The reason is that as the size of the system increases, the typical level spacing of the unperturbed Hamiltonian $\hat{H}_a+\hat{H}_b$ decreases exponentially, and the value of $|U_{ab}|$ needs to be accordingly small to validate the discussion. Second, Figs. 1–3 reveal that as U_{ab} is turned on, the level spacing statistics transform from the Poisson statistics (feature of integrable systems) to the Wigner-Dyson statistics (feature of nonintegrable systems), and at the same time the distribution of p_n heals from the triangular distribution to the Boltzmann distribution. A natural question is then, does the first transition imply or even ensure the second?

This turns out to be an intricate problem. First of all, one should note that the level spacing distribution is solely a property of the quenched Hamiltonian. Yet, the problem of thermalization depends also on the initial state of the system. In particular, here it depends on the initial temperatures of the two components. From this point of view, the level spacing distribution being the Wigner-Dyson distribution does not guarantee thermalization, since the canonical fitting worsens in the low temperature limit as mentioned above.

However, the level spacing distribution being Wigner-Dyson does seem to be a favorable, if not necessary condition of thermalization. It is generally believed that non-Wigner-Dyson distribution signals integrability or symmetry and thermalization is hampered by them. Indeed, as we shall see in Fig. 5, deviation from the Wigner-Dyson distribution in the presence of symmetry is accompanied by deterioration of the canonical fitting. Yet, levels belonging to the same symmetry class still satisfy the Wigner-Dyson distribution, and, interestingly, each class admits a good canonical fitting individually even though such a global fitting is impossible.

C. Distances and fidelities

Figure 1 gives us an overall impression of $\bar{\rho}^{(q)}$. To characterize it further, we use the tools of *distance* and *fidelity* to study its relation to some reference density matrices. The three reference density matrices chosen are, respectively, the canonical ensemble one mentioned above, the product state (q section, actually) $\rho_{\rm prod}^{(q)}(\beta_f)=\mathcal{N}_1\oplus_{q_a=0}^{M-1}e^{-\beta_f\hat{H}_a^{(q_a)}}\otimes e^{-\beta_f\hat{H}_b^{(q-q_a)}}$, and the initial density matrix $\rho^{(q)}(0)=\mathcal{N}_2\oplus_{q_a=0}^{M-1}e^{-\beta_a\hat{H}_a^{(q_a)}}\otimes e^{-\beta_b\hat{H}_b^{(q-q_a)}}$, where $\mathcal{N}_{1,2}$ are normalization coefficients such that $\mathrm{tr}(\rho_{\rm prod}^{(q)})=\mathrm{tr}[\rho^{(q)}(0)]=1$. The distance and fidelity between two density matrices are defined as $D(\rho,\sigma)=\frac{1}{2}\mathrm{tr}\sqrt{(\rho-\sigma)^2}$ and $F(\rho,\sigma)=\mathrm{tr}\sqrt{\rho^{1/2}\sigma\rho^{1/2}}$, respectively. They both take values in the range of $[0,1]$ and are closely related to each other by the inequality $1-F\leqslant D\leqslant\sqrt{1-F^2}$ [15]. Two density matrices are close to each other if the distance D and the infidelity $1-F$ are much smaller than unity.

1. General behavior

In Figs. 4(a) and 4(b), the D's and F's are shown as the interaction strength U_{ab} is varied while all other parameters fixed. We see that in the full range of U_{ab} investigated, $\rho_c^{(q)}$

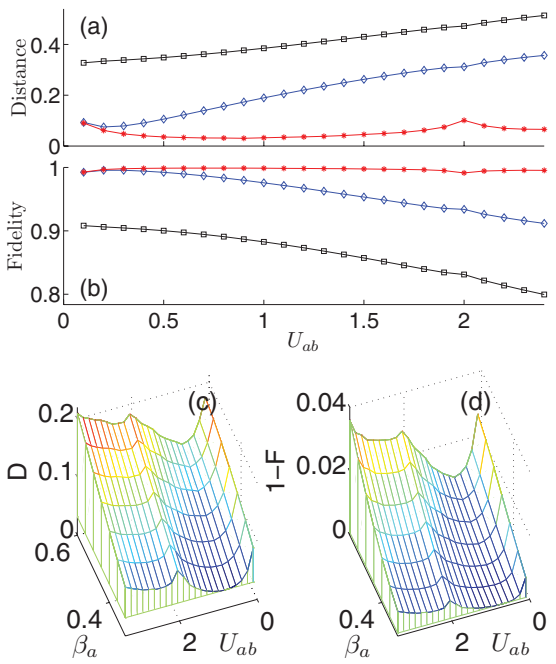

FIG. 4. (Color online) (a) Distance and (b) fidelity between $\bar{\rho}^{(q)}$ and the canonical ensemble density matrix $\rho_c^{(q)}$ (red $*$), product density matrix $\rho_{\rm prod}^{(q)}$ (blue $\diamond$), and the initial density matrix $\rho^{(q)}(0)$ (black $\square$). The parameters are $(N_a,N_b,M,q)=(4,4,9,1)$, $(J_a,J_b,U_a,U_b)=(1,1,2,2)$, and $(\beta_a,\beta_b)=(0.3,0.8)$. (c) and (d) Distance and fidelity between $\bar{\rho}^{(q)}$ and $\rho_c^{(q)}$ as functions of both the intercomponent interaction strength U_{ab} and the inverse temperatures $\beta_{a,b}$. Note that $\beta_b/\beta_a=8/3$ as β_a varies.

is the one closest to $\bar{\rho}^{(q)}$, while $\rho^{(q)}(0)$ is the farthest [and so is $\rho^{(q)}(t)$, actually, because $D(\rho^{(q)}(0),\bar{\rho}^{(q)}) = D(\rho^{(q)}(t),\bar{\rho}^{(q)})$ and $F(\rho^{(q)}(0),\bar{\rho}^{(q)}) = F(\rho^{(q)}(t),\bar{\rho}^{(q)})$ by the unitary invariance of D and F], with $\rho^{(q)}_{\rm prod}$ being the intermediate one. Moreover, the distance and infidelity between $\bar{\rho}^{(q)}$ and $\rho^{(q)}_c$ are much smaller than unity throughout the range. This indicates that the initially nonequilibrium state is effectively thermalized by time-averaging. The fact that $\rho^{(q)}_c$ is always a better approximation of $\bar{\rho}^{(q)}$ than $\rho^{(q)}_{\rm prod}$ indicates that the two subsystems equilibrate as a whole instead of factorizably. This is consistent with the fact that the intercomponent interaction is a bulk type not a surface type. We also observe that in the limit of $U_{ab} \to 0$, $D(\bar{\rho}^{(q)},\rho^{(q)}(0))$ does not converge toward zero, nor does $F(\bar{\rho}^{(q)},\rho^{(q)}(0))$ converge toward unity. The reason lies in that in the symmetric case (i.e., $J_a = J_b$, $U_a = U_b$, and $N_a = N_b$), an infinitesimal U_{ab} is enough to lift the level degeneracies and render $\bar{\rho}^{(q)}$ different from $\rho^{(q)}(0)$. This is easily seen from Eqs. (5) and (6). In the asymmetric case (e.g., $N_a \neq N_b$), when the degeneracy lift mechanism is missing, $D(\bar{\rho}^{(q)},\rho^{(q)}(0))$ and $1 - F(\bar{\rho}^{(q)},\rho^{(q)}(0))$ do converge toward zero as $U_{ab} \to 0$.

Having established the fact that $\rho^{(q)}_c$ is the best approximation of $\bar{\rho}^{(q)}$, we proceed to study the distance and fidelity between them as functions of both U_{ab} and $\beta_{a,b}$. The results are shown in Figs. 4(c) and 4(d). We see that as the initial temperatures $1/\beta_{a,b}$ are lowered, both D and $1 - F$ increase. This is in accord with what was mentioned before, that the fitting worsens in the low temperature limit. As for the intercomponent interaction strength U_{ab}, an observation is that there is a finite (optimal) value of U_{ab} ($\simeq 0.85$) where both D and $1 - F$ are at their minima. This effect is reasonable. If U_{ab} is too small, we have situations like that in Fig. 3; if U_{ab} is too large, again bad fitting is expected, since the large U_{ab} limit is an integrable limit. Indeed, it is observed in a variety of systems that thermalization is absent if the quench amplitude is too large [7,8,11,13,20].

2. *A special point: A hidden symmetry*

A curiosity invoking phenomenon revealed in Figs. 4(a) and 4(b) and further confirmed in Figs. 4(c) and 4(d) is that at $U_{ab} = 2$, there is a cusp in the values of D and F. It is interesting that D and F do not vary smoothly as functions of U_{ab}. We have looked into the time-averaged density matrix $\bar{\rho}^{(q)}$ and the level spacing distribution in the vicinity of $U_{ab} = 2$. Three values of U_{ab}, i.e., $U_{ab} = 2$, 2 ± 0.2, are investigated (see Fig. 5). We see that at the point $U_{ab} = 2$ (middle panels), the level spacing distribution deviates significantly away from the Wigner-Dyson distribution and the fluctuation of p_n is large. However, as U_{ab} moves away from this point, left or right, the Wigner-Dyson distribution is quickly recovered and the fluctuation of p_n shrinks apparently. The fact that the fluctuation of p_n is larger at $U_{ab} = 2$ than on the two sides is consistent with the fact that D and $1 - F$ are at their (local) maxima there.

It turns out that the anomaly at $U_{ab} = 2$ is rooted in the symmetry of the Hamiltonian $\hat{H}_{t>0}$ at this special point. When $J_a = J_b = J$ and $U_a = U_b = U_{ab} = U$, the total Hamiltonian is of the form

$$\hat{H}_{t>0} = -J\sum_{m=1}^{M}(\hat{a}_m^\dagger\hat{a}_{m+1} + \hat{b}_m^\dagger\hat{b}_{m+1} + \text{H.c.}) + \frac{U}{2}\sum_{m=1}^{M}[(\hat{a}_m^\dagger\hat{a}_m + \hat{b}_m^\dagger\hat{b}_m)^2 - (\hat{a}_m^\dagger\hat{a}_m + \hat{b}_m^\dagger\hat{b}_m)]. \quad (9)$$

The four operators below commute with $\hat{H}_{t>0}$:

$$\hat{N} = \sum_{m=1}^{M}(\hat{a}_m^\dagger\hat{a}_m + \hat{b}_m^\dagger\hat{b}_m), \quad (10a)$$

$$\hat{L}_z = \frac{1}{2}\sum_{m=1}^{M}(\hat{a}_m^\dagger\hat{a}_m - \hat{b}_m^\dagger\hat{b}_m), \quad (10b)$$

$$\hat{L}_+ = \sum_{m=1}^{M}\hat{a}_m^\dagger\hat{b}_m, \quad \hat{L}_- = \sum_{m=1}^{M}\hat{b}_m^\dagger\hat{a}_m. \quad (10c)$$

As the notation suggests, the three operators $\hat{L}_z$ and $\hat{L}_\pm$ satisfy the su(2) algebra, which is easily seen using the Schwinger representation of angular momentum operators. They are the sum of the corresponding components of M independent spins and they all commute with the operator

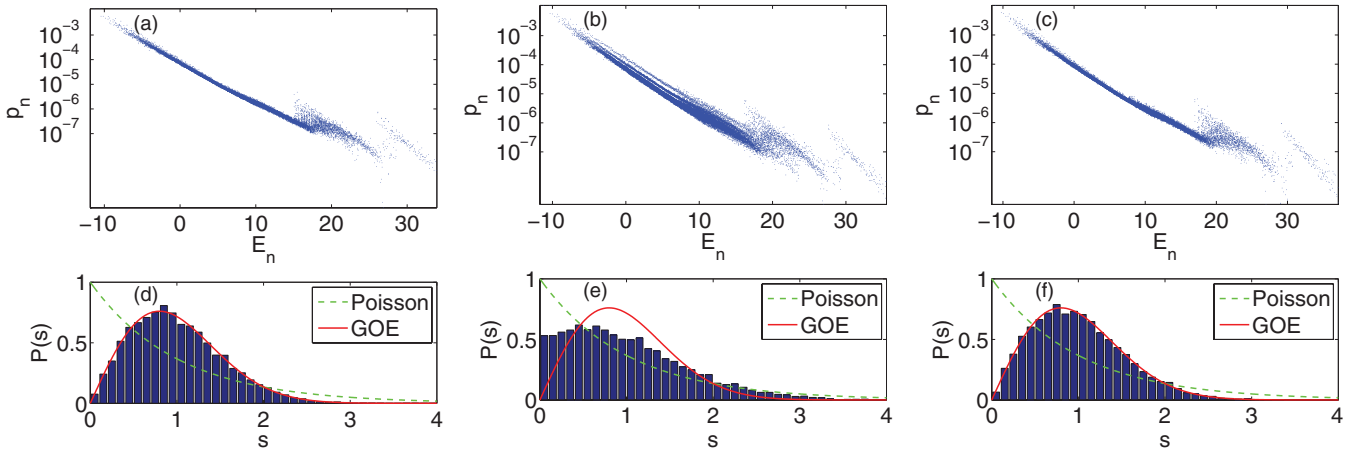

FIG. 5. (Color online) Upper panels: diagonal elements of $\bar{\rho}^{(q)}$ versus the eigenvalues of $\hat{H}^{(q)}_{t>0}$. Lower panels: level spacing distribution of $\hat{H}^{(q)}_{t>0}$. The parameters are the same as in Fig. 4(a), except that $U_{ab} = 1.8$, 2, and 2.2 in the left, middle, and right panels, respectively.

$\hat{N}$. Moreover, it is obvious that all four operators above, as the Hamiltonian $\hat{H}_{t>0}$, are invariant under the translation $(\hat{a}_m,\hat{b}_m) \to (\hat{a}_{m+1},\hat{b}_{m+1})$. This means they conserve the total quasimomentum. Therefore, the Hamiltonian $\hat{H}^{(q)}_{t>0}$ has SU(2) $\otimes$ U(1) symmetry and its eigenstates can be classified according to the irreducible representations of the group SU(2) $\otimes$ U(1). That is, each eigenstate can be labeled with a set of quantum numbers (N,L,L_z), with N, $L(L+1)$, and L_z being, respectively, the eigenvalues of the operators $\hat{N}$, $\hat{L}^2 = \hat{L}_z^2 + \frac{1}{2}(\hat{L}_+\hat{L}_- + \hat{L}_-\hat{L}_+)$, and $\hat{L}_z$. The point is that eigenstates belonging to the same set of quantum numbers do not mix as J and U vary [21].

In the specific space with fixed N_a and N_b, the values of N and L_z are fixed and, therefore, the only variable left is L. It is clear that $|N_a - N_b| = |L_z| \leqslant L \leqslant N/2 = (N_a + N_b)/2$. The second inequality is from the fact that the total spin of a collection of spins is upper bounded by the sum of the values of the spins. We have thus classified the eigenstates according to the value of L (see Appendix A) and reexamined the populations p_n and the level spacing distribution in Figs. 5(b) and 5(e), respectively. The results are presented in Fig. 6. There, in the left panel, a close-up of Fig. 5(b) is shown, but with eigenstates of different values of L differentiated by different colors. The interesting fact revealed is that each set of dots form a narrow stripe, and the stripes run almost parallel to each other. The point is that each L class admits a good canonical fitting individually, though the classes as a whole can not be fitted well. It seems that thermalization is robust within each symmetry class even if it cannot maintain itself globally. This effect constitutes an impressive scenario of how symmetry of the Hamiltonian may affect thermalization of a system. We have also studied other q subspaces and superposed Fig. 6(a) with different q's. The resulting figure is quite similar to Fig. 6(a).

It is instructive to compare Fig. 6(a) with Fig. 1(c), where there is no appreciable difference between different q classes. In contrast, in Fig. 6(a) the displacements between the L classes are quite remarkable. Whether this is just a finite-size effect and the offsets between the L classes will disappear

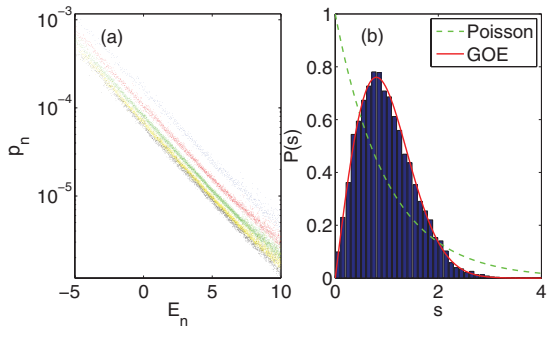

FIG. 6. (Color online) Left panel: a close-up of Fig. 5(b). From up to down, the blue, red, green, yellow, and black dots correspond to eigenstates with total angular momentum $L = 4$, 3, 2, 1, and 0, respectively. Note that each set of dots form a narrow stripe. Right panel: level spacing distribution of the Hamiltonian $\hat{H}^{(q)}_{t>0}$. The parameters are the same as in Figs. 5(b) and 5(e). But in contrast to Fig. 5(e), only eigenvalues with $L = 2$ [green dots in (a)] are taken.

in the thermodynamic limit is unclear currently and is up to future work.

D. Equilibration of physical variables and the role of the eigenstate thermalization hypothesis

It has been verified in many aspects that $\bar{\rho}^{(q)}$ can be well approximated by some canonical ensemble density matrix $\rho_c^{(q)}(\beta_f)$. We then anticipate that the time-averaged values (predicted by $\bar{\rho}^{(q)}$) of many physical quantities of interests are also well predicted by $\rho_c^{(q)}$. Moreover, if dephasing is effective, we shall see perfect relaxation phenomenon in the dynamics of the physical quantities. It is indeed the case. As shown in Fig. 7(a), occupations on the Bloch modes $\langle\hat{a}_k^\dagger\hat{a}_k\rangle$ [and $\langle\hat{b}_k^\dagger\hat{b}_k\rangle$] relax to their average values quickly, exhibiting minimal fluctuations [13,22], and these values are very close to those predicted by $\rho_c^{(q)}$ (but with much larger discrepancy to those by the microcanonical ensemble density matrix $\rho_{\rm mic}^{(q)}$ [23]). That is, these quantities relax and relax to their equilibrium values in $\rho_c^{(q)}$. Note that due to the symmetric parameters chosen, $\langle\hat{a}_k^\dagger\hat{a}_k\rangle = \langle\hat{b}_k^\dagger\hat{b}_k\rangle$ for $\bar{\rho}^{(q)}$, $\rho_c^{(q)}$, and $\rho_{\rm mic}^{(q)}$ all, and indeed in Fig. 7(a), $\langle\hat{a}_k^\dagger\hat{a}_k\rangle$ and $\langle\hat{b}_k^\dagger\hat{b}_k\rangle$ merge from distinct initial values.

Here, some remarks about the connection between thermalization of the density matrix and that of physical observables are in order. The point is that the former implies, but is unnecessary for, the latter. Two density matrices can yield the same expectation values for a few "realistic" physical quantities, yet be quite far apart in terms of D and F. Actually, for a generic system, in the thermodynamic limit, the predictions of a microcanonical ensemble and a canonical one agree, yet it is easy to persuade oneself that the distance and fidelity between the corresponding density matrices are such that $(1 - D, F) \ll 1$. The reason is formulated as the eigenstate thermalization hypothesis (ETH) [24], which is verified in some finite systems [9,10]. According to ETH, the expectation value of a generic few-body physical quantity varies little between eigenstates close in energy; therefore, the detailed distribution p_n does not matter as long as it is narrow in energy. Here, it is verified that ETH is acceptable for the variables in Fig. 7(a) [see Fig. 7(b)]. However, it plays a marginal role in the thermalization of the physical observables there. As shown in Fig. 7(b), the average energy $\bar{E}$ falls at the head of the spectrum where ETH is not so good. Thus, we see in Fig. 7(a) that the predictions of $\rho_{\rm mic}^{(q)}$ deviate significantly from the true values, yet the predictions of $\rho_c^{(q)}$ agree much better with $\bar{\rho}^{(q)}$. This situation persists in a wide range of parameters, even if $\bar{E}$ falls in the body of the spectrum where ETH is good. It is thus apparent that in our case it is the detailed distribution, which is more accurately captured by $\rho_c^{(q)}$ than $\rho_{\rm mic}^{(q)}$, that really matters. However, this does not rule out the possibility that in the thermodynamic limit, the distribution of E falls in a small interval where ETH holds and thus both $\rho_c^{(q)}$ and $\rho_{\rm mic}^{(q)}$ agree with $\bar{\rho}^{(q)}$ as the physical observables are concerned.

Here, an issue needs to be clarified. Figure 7(b) shows that $\bar{E}$ is on the edge of the spectrum. One may wonder how the system can thermalize with so "low" an energy. The point

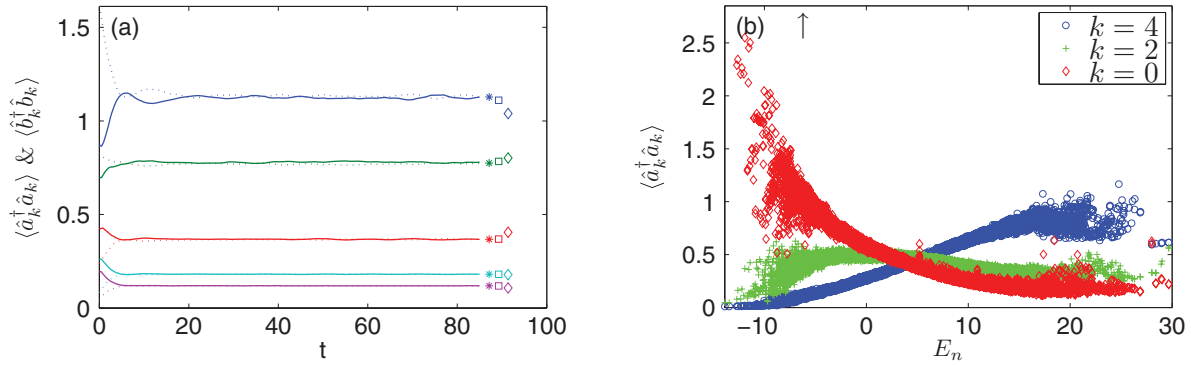

FIG. 7. (Color online) (a) Evolution of the occupations on the Bloch states, $\langle \hat{a}_k^\dagger \hat{a}_k \rangle$ (solid lines) and $\langle \hat{b}_k^\dagger \hat{b}_k \rangle$ (dotted lines). From up to down, $k = 0, \ldots, 4$. Other k's are not shown because lines with k and $M - k$ are very close to each other all the time. For each pair of lines, the markers of the same color on the right hand side indicate the $\bar{\rho}^{(q)}$ prediction ($*$), $\rho_c^{(q)}$ prediction ($\square$), and $\rho_{\rm mic}^{(q)}$ prediction ($\diamond$), respectively. The parameters are the same as in Fig. 4(a) with $U_{ab} = 1$. (b) Occupations on the Bloch states $\langle \hat{a}_k^\dagger \hat{a}_k \rangle$ for each eigenstate of $\hat{H}_{t>0}^{(q)}$. The $\uparrow$ indicates the average energy $\bar{E}$ in (a).

is that though judged by eye, $\bar{E}$ is close to the ground-state energy, it is actually located in a high density-of-state region [see Fig. 1(b)]. Thousands of levels participate significantly in $\bar{\rho}^{(q)}$. It is not the case such that only a few levels (the ground-state and some low excited levels) contribute to $\bar{\rho}^{(q)}$. Moreover, it should be noted that $\bar{E}$ is not a good indicator of the hotness or coolness of the system, because it is an extensive quantity. The final temperature (an intensive quantity) $1/\beta_f$ is. In Fig. 7, $1/\beta_f \simeq 2$, which is half of the band width of a one-dimensional tight binding model with hopping amplitude unity. This temperature is not so low.

IV. IMPLICATIONS OF THE GOOD FITTING

We now return to Fig. 1. The fact that the occupations on the eigenstates

$$p_n = \mathcal{N} \sum_{|ij\rangle \in \mathcal{H}^{(q)}} e^{-\beta_a E_a^i - \beta_b E_b^j} |\langle ij|\psi_n\rangle|^2, \tag{11}$$

where $\mathcal{N}$ is a normalization factor, are well fitted by the formula $p_n \propto e^{-\beta_f E_n}$, is too remarkable to be overlooked. This fact is consistent with the other fact that $S(\bar{\rho}^{(q)})$ is very close to $S(\rho_c^{(q)})$, as shown in the inserts of Fig. 1. Because the canonical distribution is the only one that maximizes the entropy when the average energy is fixed [25], $\bar{\rho}^{(q)}$ should be close to $\rho_c^{(q)}$ if $S(\bar{\rho}^{(q)}) \lesssim S(\rho_c^{(q)})$.

So far we have not fully understood this nontrivial fact, but we do understand the weak fact that $p_n/p_m \simeq 1$ if $|E_n - E_m| \ll 1/\beta_f$, in particular, $p_n/p_{n+1} \simeq 1$. That is, the populations on two eigenstates are close if the eigenenergies are close. We have

$$p_n = \mathcal{N} \int \int_{-\infty}^{+\infty} dE_a dE_b P_n(E_a, E_b) e^{-\beta_a E_a - \beta_b E_b}, \tag{12}$$

with the probability distribution function $P_n(E_a, E_b) = \sum_{|ij\rangle} |\langle ij|\psi_n\rangle|^2 \delta(E_a - E_a^i, E_b - E_b^j)$ [26]. It consists of a series of δ functions with fixed positions but n-dependent amplitudes and is an *intrinsic* property of $|\psi_n\rangle$ in terms of $|ij\rangle$. Coarse-graining P_n by replacing the δ functions with some regular peaked function $f(x,y)$ (satisfying $\int \int dxdyf = 1$ and $f > 0$), we rewrite p_n as

$$p_n = \frac{\mathcal{N}}{c} \int \int_{-\infty}^{+\infty} dE_a dE_b \bar{P}_n(E_a, E_b) e^{-\beta_a E_a - \beta_b E_b}. \tag{13}$$

Here, the coarse-grained distribution $\bar{P}_n(E_a, E_b) = \sum_{|ij\rangle} |\langle ij|\psi_n\rangle|^2 f(E_a - E_a^i, E_b - E_b^j)$, and the constant $c = \int \int dxdy e^{-\beta_a x - \beta_b y} f(x,y)$, which is n-independent. The fact that $\bar{\rho}^{(q)}$ and $\rho_c^{(q)}$ in Fig. 1 always agree well in the high-temperature regime $\beta_{a,b} \leqslant 0.4$ suggests that there exists some f such that for most n's, $\bar{P}_n$ and $\bar{P}_{n+1}$ are close to each other in a certain sense—an *intrinsic* property independent of $\beta_{a,b}$. As a measure of the difference between two distributions, we have the metric [15]

$$\|\bar{P}_n - \bar{P}_m\| \equiv \frac{1}{2} \int \int_{-\infty}^{+\infty} dE_a dE_b |\bar{P}_n - \bar{P}_m|. \tag{14}$$

By this metric, two distributions are close to each other if $\|\bar{P}_n - \bar{P}_m\| \ll 1$. We have studied the distances between $\bar{P}_n$ and $\bar{P}_{n+1}$ using the Gaussian function $f(x,y) = \frac{1}{\pi w^2} \exp[-(x^2 + y^2)/w^2]$, where w is the adjustable width. The results are shown in Fig. 8. We see that although for the initial distributions ($w = 0$, in this case $\bar{P}_n$ degenerates to P_n), $\|\bar{P}_n - \bar{P}_{n+1}\|$ centers around 0.63, once broadening is triggered, it shrinks abruptly. For $w = 0.5$ and 1, over 84% and 93% pairs have a distance less than 0.1, respectively. Moreover, those pairs having large distances fall mainly at the ends of the spectrum, consistent with the fact that in Fig. 1 the fitting is bad at the ends (large fluctuations). In Figs. 8(c)–8(f), the broadened distributions $\bar{P}_n(E_a, E_b)$ for four successive n's are illustrated. It is apparent that they agree even in detail. We also observe that the contour of $\bar{P}_n$ stretches along the direction $E_a + E_b =$ const. This is reasonable since $\hat{H}_{ab}$, as a perturbation, mixes eigenstates of $\hat{H}_a + \hat{H}_b$ with adjacent eigenenergies best. At this point, we can understand why the fitting in Fig. 1 is good and why low temperature and large difference $|\beta_a - \beta_b|$ are adverse for the fitting. The exponential weight function $e^{-\beta_a E_a - \beta_b E_b}$ descends fastest in the direction (β_a, β_b). In the two adverse conditions, the weight function changes significantly across the region where $\bar{P}_n$ takes significant values and which

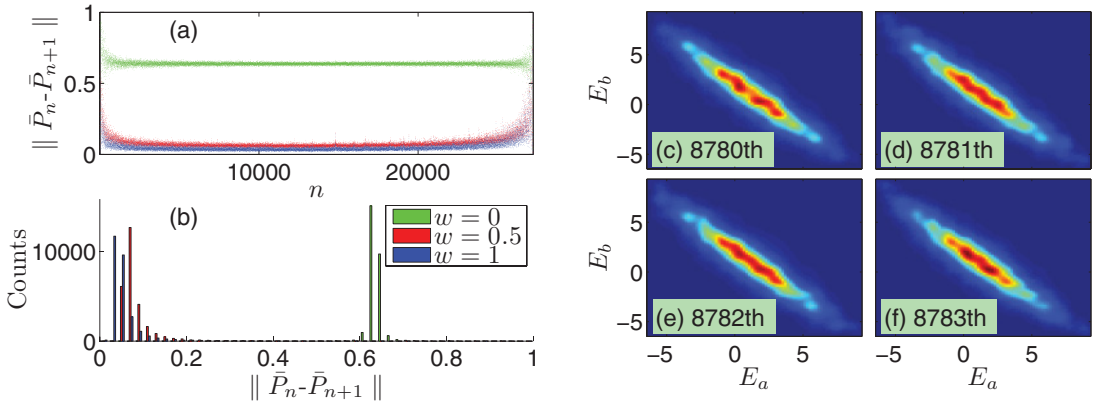

FIG. 8. (Color online) (a) Distances between coarse-grained probability distributions corresponding to adjacent eigenstates, with Gaussian broadening. The green, red, and blue dots correspond to $w = 0$, 0.5, and 1, respectively. (b) Histogram of $\|\bar{P}_n - \bar{P}_{n+1}\|$ in bins of length 0.02. (c)–(f) illustrate the Gaussian broadened ($w = 0.5$) probability distributions corresponding to four successive eigenstates. The distances between adjacent pairs are (0.0460,0.0419,0.0502). The parameters are the same as described in the caption of Fig. 1(b) (but note that $\beta_{a,b}$ are irrelevant here).

extends primarily in the direction $(1, -1)$. This nonuniformity potentially will spoil the closeness between $\bar{P}_n$ and $\bar{P}_{n+1}$ in terms of the metric above.

Finally, we should mention that the essence of coarse-graining is to smear out irrelevant details of the distribution P_n and retain only the relevant overall information. To be specific, since $e^{-\beta_a E_a - \beta_b E_b}$ is a smooth function of $E_{a,b}$, p_n is sensitive not to the individual amplitudes of δ functions located near each other but only to the average amplitude of them. As the system size grows, the number of δ functions within the radius w increases exponentially and coarse-graining shall be even more effective in reducing the distance between P_n and P_{n+1}, and therefore it is legitimate to expect even better fitting.

So far we have been dealing with the good fitting case in Fig. 1. We now turn to the interesting case in Fig. 5(b). There the fluctuation of p_n among eigenstates from different L classes is relatively large, while the fluctuation of p_n within each individual L class is much smaller. This indicates that the difference between the coarse-grained probability distributions of eigenstates from different L classes is relatively large, yet much smaller within each L class. It is indeed the case. In Fig. 9(a), the distances $\|\bar{P}_n - \bar{P}_{n+1}\|$ are shown. We see that, in contrast to that in Fig. 8(a), even under coarse graining, a significant portion of $\|\bar{P}_n - \bar{P}_{n+1}\|$ remain large. However, if we pick out a specific L class and study the distance $\|\bar{P}_n^{(L)} - \bar{P}_{n+1}^{(L)}\|$ again, the good case in Fig. 8(a) reappears. Here, $\bar{P}_n^{(L)}$ refers to the coarse-grained probability distribution of the nth eigenstate in the L class.

A notable fact in Figs. 8(a) and 9(b) is that the distances (green dots) between the non-coarse-grained probability distributions $\bar{P}_n$ and $\bar{P}_{n+1}$ (or $\bar{P}_n^{(L)}$ and $\bar{P}_{n+1}^{(L)}$) concentrate around some value ($\simeq 0.637$). This is not accidental. It is actually consistent with the fact that the level spacing distribution is Wigner-Dyson [see Figs. 2(b) and 6(b)], which is a characteristic of the GOE of hermitian matrices [27]. We have drawn

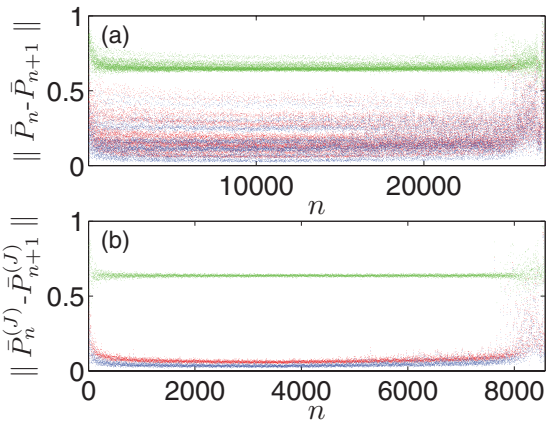

FIG. 9. (Color online) (a) Distances between coarse-grained probability distributions corresponding to adjacent eigenstates, with Gaussian broadening. The green, red, and blue dots correspond to $w = 0$, 0.5, and 1, respectively. The parameters are the same as described in the caption of Fig. 5(b). (b) Similar to (a) but only adjacent eigenstates belonging to the $L = 2$ class are considered.

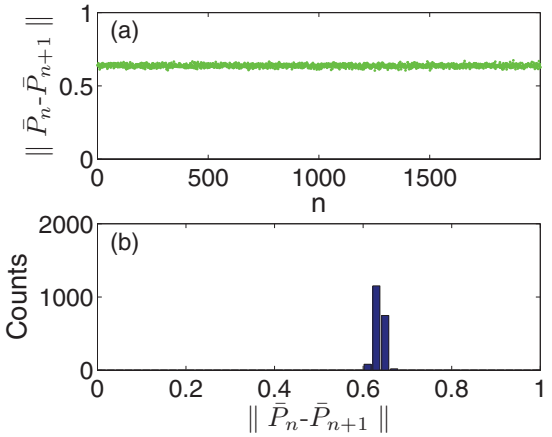

FIG. 10. (Color online) (a) Distances between the probability distributions [see Eq. (15)] corresponding to adjacent eigenstates of a 2000×2000 matrix drawn from the Gaussian orthogonal ensemble. (b) Histogram of $\|\bar{P}_n - \bar{P}_{n+1}\|$ in bins of length 0.02.

a $d \times d$ ($d = 2000$) hermitian matrix h from this ensemble numerically. Denote the nth (normalized) eigenvector of h as $\vec{v}_n = (v_{1n}, v_{2n}, \ldots, v_{dn})^T$. The counterpart of Eq. (14) is

$$\|\bar{P}_n - \bar{P}_m\| \equiv \frac{1}{2}\sum_{i=1}^{d} \left|v_{in}^2 - v_{im}^2\right|. \tag{15}$$

The statistics of $\|\bar{P}_n - \bar{P}_{n+1}\|$ are shown in Fig. 10. We see that the behavior in Figs. 8(a), 8(b), and 9(b) is recovered quantitatively. This demonstrates the presence of universality in the system in question. In Appendix B, we will give a tentative account of the typical value 0.637 of $\|\bar{P}_n - \bar{P}_{n+1}\|$ in the non-coarse-grained case.

V. CONCLUSIONS

To conclude, it is demonstrated that the generic two-component Bose-Hubbard model can exhibit perfect thermalization at finite temperatures and appropriate parameters. It is strong thermalization in that not merely the average values of a few physical variables but even the time-averaged density matrix of the whole system itself thermalizes. Our finding constitutes an interesting, (so far) isolated example in regard to the mechanism of thermalization. There is concern that thermalization of the density matrix itself, especially the density matrix of the whole system, may be too strong to be a general mechanism of thermalization. Indeed, first, at least in some other systems [10], this is unnecessary and some other mechanism can account for thermalization of the physical observables. Second, existing theories can predict canonical behavior for subsystems only. However, since the problem of thermalization is yet largely open, one should be open-minded to welcome the possibility that thermalization does happen in its strong form in some circumstances. Hopefully this issue can be solved in future work.

We have also identified the influence of symmetry on thermalization. An empirical observation is that levels belonging to the same symmetry class share the same fate or feature with each another, while levels from different classes are less correlated. This point is reflected in several aspects. First, levels in the same symmetry class couple with each another and they show level repulsion and Wigner-Dyson statistics. On the contrary, levels in different classes do not couple and it is okay for them to get close to each other or even cross each other, which results in Poisson-like statistics. Second, in the presence of SU(2) symmetry, it is observed that levels within each L class coordinate themselves in such a way to satisfy the canonical distribution very well, while different L classes are seemingly independent. Third, the coarse-grained probability distributions of levels in the same L class are close to each another as long as the levels are close in energy, yet those of levels in different L classes are far from each another even if the energies are close. Overall, the lesson is that symmetry, like integrability, hampers thermalization; and breaking symmetry, like breaking integrability, favors thermalization.

Note added in proof. Recently, an account of the "strong thermalization" observed here was given by Ponomarev *et al.* in Ref. [28].

ACKNOWLEDGMENTS

We are grateful to L. M. Duan and J. P. Hu for helpful discussions, and F. C. Cui for lending us the computational resources. J.M.Z. is supported by NSFC Grant No. 11091240226.

APPENDIX A: NUMBER OF LEVELS IN AN L CLASS

The number of levels within an L class can be related to the dimension of the Hilbert space with fixed (N_a, N_b, q) [denoted as $D^{(q)}(N_a, N_b)$, with the dependence on M suppressed] in a simple way. Using the raising and lowering operators $\hat{L}_\pm$, we see that there is a one-to-one correspondence between levels of the same value of L but different values of L_z or (N_a, N_b) (but with $N_a + N_b = N$ fixed). Therefore, we have

$$D^{(q)}(N_a, N_b) = \sum_{L=|N_a-N_b|}^{L=N} n_L^{(q)}(N), \tag{A1}$$

where $n_L^{(q)}(N)$ is the number of levels in the L class, which depends on the value of N but not on $N_a - N_b$. From Eq. (A1), we have then

$$\begin{aligned} n_L^{(q)}(N) = {} & D^{(q)}\left(\tfrac{1}{2}(N+L), \tfrac{1}{2}(N-L)\right) \\ & - D^{(q)}\left(\tfrac{1}{2}(N+L)+1, \tfrac{1}{2}(N-L)-1\right). \end{aligned} \tag{A2}$$

APPENDIX B: A TENTATIVE ACCOUNT OF THE TYPICAL VALUE

It is stimulating and enlightening to give a tentative account of the typical value 0.637 in Sec. IV. For the GOE, each eigenvector (referred to by the rank of the corresponding eigenvalue within the spectrum) satisfies the uniform (rotationally invariant) distribution on the hypersphere $S_{d-1} : \sum_{i=1}^{d} x_i^2 = 1$. This distribution can be realized by generating d independent, normally distributed random variables $\vec{x} = (x_1, x_2, \ldots, x_d)$, and then taking the projection $\vec{x} \to \hat{x} \equiv \vec{x}/\|\vec{x}\|$, with $\|\vec{x}\| = (\sum_{i=1}^{d} x_i^2)^{1/2}$. Suppose we sample two points $\hat{x}$ and $\hat{y}$ on the hypersphere S_{d-1} according to this algorithm. Now, consider the metric similar to Eq. (15):

$$m(\hat{x}, \hat{y}) = \frac{1}{2}\sum_{i=1}^{d} \left| \frac{x_i^2}{\|\vec{x}\|^2} - \frac{y_i^2}{\|\vec{y}\|^2} \right|. \tag{B1}$$

For d large enough, according to the large number law, the typical value of $\|\vec{x}\|^2$ and $\|\vec{y}\|^2$ is d. Therefore, $m(\hat{x}, \hat{y})$ can be well approximated by $\frac{1}{2d}\sum_{i=1}^{d} |x_i^2 - y_i^2|$. Here, x_i and y_i are independent, normally distributed random variables. Using the large number law again, we get readily that the typical value of $m(\hat{x}, \hat{y})$ can be well approximated by

$$\begin{aligned} \frac{1}{2}\overline{\left|x_i^2 - y_i^2\right|} &= \frac{1}{4\pi}\int\int_{-\infty}^{+\infty} dx_i dy_i e^{-\frac{1}{2}(x_i^2+y_i^2)}\left|x_i^2 - y_i^2\right| \\ &= \frac{2}{\pi} \simeq 0.637. \end{aligned} \tag{B2}$$

That is, if we choose two unit vectors on the hypersphere S_{d-1} independently and according to the uniform distribution, with probability approaching unity, the metric between them as defined in Eq. (B1) will be very close to the value 0.637. This final conclusion has been verified numerically using the algorithm above.

Here, we have assumed the two unit vectors to be independent. This is definitely not the case for two eigenvectors of a Hamiltonian drawn from the GOE, since they must be orthogonal to each other. However, this should not be a great limitation. The two unit vectors drawn in the way above, with probability very close to unity, are nearly orthogonal since the expectation value of the square of the inner product between them is $1/d$ [29]. Therefore, it is believed that the simplified problem considered above is the essential mechanism for the typical value 0.637 observed in Sec. IV.

[1] J. Gemmer, M. Michel, and G. Mahler, *Quantum Thermodynamics*, 2nd ed. (Springer, Berlin, 2009).

[2] E. Fermi, J. R. Pasta, and S. Ulam, Los Alamos Scientific Laboratory Report No. LA-1940, May 1955.

[3] N. J. Zabusky and M. D. Kruskal, Phys. Rev. Lett. **15**, 240 (1965).

[4] T. Kinoshita, T. Wenger, and D. S. Weiss, Nature (London) **440**, 900 (2006).

[5] M. A. Cazalilla, Phys. Rev. Lett. **97**, 156403 (2006).

[6] M. Rigol, V. Dunjko, V. Yurovsky, and M. Olshanii, Phys. Rev. Lett. **98**, 050405 (2007).

[7] S. R. Manmana, S. Wessel, R. M. Noack, and A. Muramatsu, Phys. Rev. Lett. **98**, 210405 (2007).

[8] C. Kollath, A. M. Lauchli, and E. Altman, Phys. Rev. Lett. **98**, 180601 (2007).

[9] M. Rigol, Phys. Rev. Lett. **103**, 100403 (2009).

[10] M. Rigol, V. Dunjko, and M. Olshanii, Nature (London) **452**, 854 (2008); M. Rigol, Phys. Rev. A **82**, 037601 (2010).

[11] G. Roux, Phys. Rev. A **79**, 021608(R) (2009).

[12] J. Gemmer and M. Michel, Europhys. Lett. **73**, 1 (2006); J. Gemmer and G. Mahler, Eur. Phys. J. B **31**, 249 (2003).

[13] J. M. Zhang, C. Shen, and W. M. Liu, Phys. Rev. A **83**, 063622 (2011).

[14] This statement should not be confused with the statement that $\langle \hat{O} \rangle$ as a function of time decays exponentially to its steady value.

[15] M. A. Nielsen and I. L. Chuang, *Quantum Computation and Quantum Information* (Cambridge University Press, Cambridge, 2000).

[16] J. M. Zhang and R. X. Dong, Eur. J. Phys. **31**, 591 (2010).

[17] Similar behavior is observed in A. V. Ponomarev, S. Denisov, and P. Hänggi, Phys. Rev. Lett. **106**, 010405 (2011). But there it is about subsystems (reduced density matrices).

[18] V. K. B. Kota, Phys. Rep. **347**, 223 (2001); V. Zelevinsky, B. A. Brown, N. Frazier, and M. Horoi, *ibid.* **276**, 85 (1996).

[19] A. Gubin and L. F. Santos, e-print arXiv:1106.5557; L. F. Santos and M. Rigol, Phys. Rev. E **81**, 036206 (2010).

[20] M. Rigol and L. F. Santos, Phys. Rev. A **82**, 011604(R) (2010).

[21] J. F. Cornwell, *Group Theory in Physics: An Introduction* (Elsevier, Singapore, 2006).

[22] P. Reimann, Phys. Rev. Lett. **101**, 190403 (2008); N. Linden, S. Popescu, A. J. Short, and A. Winter, Phys. Rev. E **79**, 061103 (2009).

[23] Defined as $\rho_{\rm mic}^{(q)} = \frac{1}{\mathcal{N}} \sum_{|\psi_n\rangle \in \mathcal{H}^{(q)}, |E_n - \bar{E}| \leqslant 0.4} |\psi_n\rangle\langle\psi_n|$.

[24] J. M. Deutsch, Phys. Rev. A **43**, 2046 (1991); M. Srednicki, Phys. Rev. E **50**, 888 (1994).

[25] E. T. Jaynes, Phys. Rev. **106**, 620 (1957).

[26] It is so called because $\iint dE_a dE_b P_n(E_a, E_b) = 1$ and $P_n(E_a, E_b) \geqslant 0$.

[27] M. L. Mehta, *Random Matrices*, 3rd edition (Elsevier, Singapore, 2006).

[28] A. V. Ponomarev, S. Denisov, J. Gemmer, and P. Hänggi, e-print arXiv:1107.6013.

[29] S. Goldstein, J. L. Lebowitz, R. Tumulka, and N. Zanghì, Phys. Rev. Lett. **96**, 050403 (2006).